A 5-GHz high-temperature superconducting reaction-type transmitting filter based upon split open-ring resonators

S Futatsumori[1], T Hikage[1], T Nojima[1], A Akasegawa[2], T Nakanishi[2] and K Yamanaka[2]

[1]Graduate School of Information Science and Technology, Hokkaido University, Kita 14, Nishi 9, Kita-ku, Sapporo, Hokkaido, 060-0814, Japan

[2]Fujitsu Limited, 10-1 Morinosato-Wakamiya, Atsugi, Kanagawa, 243-0197, Japan

E-mail: `futatsumori@emwtinfo.ice.eng.hokudai.ac.jp`

Abstract. A new kind of high-temperature superconducting (HTS) transmitting filter based on a reaction-type resonator is presented. The purpose of an HTS reaction-type filter (HTS-RTF) is to eliminate the intermodulation distortion noise generated by microwave power amplifiers such as those employed in mobile base stations. An HTS-RTF enables both higher power handling capability and sharper cutoff characteristics compared to existing planar-type HTS transmitting filters, since a reaction-type resonator does not resonate with high-power fundamental signals. To achieve steep skirt characteristics and high-power handling capability simultaneously, a 5-GHz three-pole HTS-RTF using split open-ring resonator is designed. This split open-ring resonator offers low maximum current densities and a high-unloaded Q-factor with low radiation. The designed prototype filter has Chebyshev characteristics with a centre frequency of 4.95 GHz and a bandwidth of 1.5 MHz. The HTS-RTF is fabricated using a double-sided $YBa_2C_3O_{7-\delta}$ thin film deposited on a 0.5 mm thick MgO substrate. The measured filter shows an insertion loss of less than 0.1 dB and a third intermodulation distortion value of - 56.7 dBc for a 40 dBm passband signal. In addition, adjacent channel leakage power ratio (ACLR) measurements using an actual Wideband CDMA signal confirm an ACLR improvement of about 10 dB for a four-carrier signal with power of up to 40 dBm.

PACS numbers: 84.30.Vn, 84.40.Dc, 85.25.Am

Submitted to: *Supercond. Sci. Technol.*

1. Introduction

High-temperature superconducting (HTS) thin film materials enable the realization of high-performance microwave planer filters with low insertion loss, sharp skirts, and small volume at the same time. This is because the surface resistances of HTS materials are zero at direct current, and more than two orders lower than those of normal conductors even in the microwave region [1]. There have been strong efforts to develop HTS filters for practical applications such as mobile communication systems, satellite communication systems, and meteorological radar systems [2, 3, 4, 5, 6]. Unfortunately, existing HTS materials exhibit small power handling capability due to local concentrations of current density and nonlinear surface resistance (R_s), which limits their application. Nonlinear R_s causes the generation of harmonic distortion and intermodulation distortion (IMD) [7]. These distortions lead to serious problems when the devices are applied as transmitting filters [8]. This is one reason why HTS transmitting filters fail to match the performance of transmitting filters. The technical key to achieve HTS transmitting filters is to improve their power-handling capability while maintaining sharp cut off characteristics and small volumes.

In this paper, a 5-GHz HTS transmitting filter based on a reaction-type resonator is proposed. An HTS reaction-type filter (HTS-RTF) is a bandstop filter based on a reaction-type resonator; the combination aims to eliminate the intermodulation distortion noise generated by microwave power amplifiers. This paper presents the fundamental approach used to confirm HTS-RTF applicability.

First, the effectiveness of an HTS-RTF is explained by using the power amplifier output spectrum of an IMT-2000 mobile base station. We propose to use an HTF-RTF instead of the complicated and expensive nonlinear compensation circuit employed in almost all mobile base stations. Second, the reaction-type resonator used in the filter is briefly introduced. Split open-ring resonators (SORR) were previously proposed by the authors and are described in [9, 10]. The SORR structure enables the maximum current densities to be reduced while offering both high-unloaded Q-factor (Q_u) and low radiation levels. A 5-GHz three-pole HTS-RTF based on the SORR is designed to offer Chebyshev transfer functions and is fabricated. The analysis results of the filter is described in [11]. As a first step, we are focusing on the sharp skirt property and low IMD characteristics rather than filter bandwidth or the level of suppression. Next, third-order and fifth-order IMD generated by the HTS-RTF are measured using a two-tone signal. Finally, Wideband CDMA (W-CDMA) four-carrier measurements are carried out to confirm the effectiveness of the HTS-RTF. The adjacent channel leakage power ratio (ACLR) of a power amplifier with and without the HTS-RTF is measured. As far as the authors know, this is the first proposal to use an HTS bandstop filter to suppress the adjacent channel noise generated by a power amplifier.

2. Reaction-type filter and applications

The purpose of an HTS-RTF is to eliminate the intermodulation distortion noise generated by microwave power amplifiers, such as those employed in mobile base stations. An output spectrum typical of the power amplifiers used in mobile base stations is shown in figure 1. The W-CDMA four-carrier signal lies at the centre frequency. In addition, adjacent channel noises, generated by the nonlinear characteristic of the power amplifiers, lie on either side of the carrier signals. To reduce these noises, nonlinear compensation techniques such as predistortion [12] and feedfoward [13] are commonly applied to the transmission circuits. The two lines in figure 1 show the output spectrum with and without the compensation circuits. To avoid interference with other communication systems, regulations or specifications strictly limit the acceptable level of these noises [14].

A carrier signal and its adjacent channel noise are so close that conventional room temperature filters cannot be used. Considering the spectrum shown in figure 1, a filter with the very steep skirt property of more than 20 dB MHz^{-1} is required to suppress these noises. A cavity-based high-Q filter offers this performance at room temperature, however, its volume is too large to permit installation within a mobile base station. Furthermore, the insertion loss of such a cavity filter would be much higher desired. Another solution is an adjacent channel noise suppression method based on digital signal processing [15]. This method, called the clipping and filtering method, treats the base band signal. A practical HTS-RTF would be a reliable and simple solution to suppress the noise and far superior to methods based on digital signal processing. This is because an HTS-RTF treats the radio frequency signal in a direct and straightforward manner. Using an HTS-RTF with a sharp cutoff characteristic for noise suppression offer two advantages to the transmitting circuit. First, the complicated and expensive nonlinear distortion compensation circuits of the power amplifiers can be replaced by HTS-RTFs. These filters are feasible since the required value of noise suppression is 20 dB at most. Second, by reducing the noise, we can run the power amplifiers at a more power-efficient operating point. These advantages lead to transmitting circuits with high cost performance and low energy consumption.

Since the HTS-RTF described herein is a bandstop filter based on a reaction-type resonator, it does not, ideally, resonate when handling high-power fundamental signals. It reacts only to low power noise. Assuming that the fundamental signal is 40 dBm and the adjacent channel noise is -50 dBc to -40 dBc lower than the fundamental signal, see figure 1, the resonator needs to handle noise powers of just -10 dBm to 0 dBm. This is the most significant difference between a transmission-type bandpass filter and a reaction-type bandstop filter. Because of this, an HTS-RTF has the possibility of achieving both higher power handling capability and sharper cutoff characteristics than existing planar-type HTS transmitting filters.

3. Reaction-type resonator

A reaction-type resonator ideally passes the fundamental signal to the feedline and does not resonate. In 5-GHz band fabricated resonators, however, the fundamental signal does induce some current on the resonators. This induced current generates nonlinear distortion noise. In addition, the attendant decrease in Q_u values and increase in radiation energy lead to unwanted coupling effects and degrade overall performance of the filter. To overcome these problems, the split open-ring resonator (SORR) is proposed. The SORR considered here is described in more detail in previous papers [9, 10] and is only briefly touched on in this section.

The geometry of the SORR structure and the conventional open-ring resonator are shown in figure 2(a) and figure 3, respectively. As shown in figure 2(a), the SORR consists of two, opposite direction, open-ring resonators. The parallel edges of the SORR reduce the edge-current concentration. Moreover, radiation from the resonator is suppressed, because the current flows on the resonator edge have inverse direction as shown in figure 2(b). A full-wave electromagnetic analysis based on the method of moments is used to investigate the relationship between the resonant properties, the surface current densities and the structural parameters of the resonators. In the analysis, the material of the substrate is assumed to be MgO with relative dielectric constant of 9.7, the loss tangent of 5.5×10^{-6}, and the thickness of 0.5 mm, see table 1. The HTS thin-film material is assumed to be $YBa_2C_3O_{7-\delta}$ (YBCO) with conductivity of 6.5×10^{12} S/m and thickness of 0.5 μm. The resonator is modelled using the shielded box shown in figure 4.

The dimensions of the resonators are adjusted to achieve the same coupling coefficient and the same fundamental resonance frequency $f_0 = 4.95$ GHz. The input signal used in the current density calculation is a sinusoidal wave with 1 V amplitude that is 5 MHz offset from the resonance frequency. Figure 5 shows the maximum induced current density as a function of resonator gap g. When the resonator gap is wider than 0.2 mm, the maximum induced current density is lower than that of a conventional open-ring resonator. In addition, the energy radiated from the resonator is calculated by using the frequency characteristics without a shielding box [10]. Figure 6 shows the radiation quality factor (Q_r) as a function of resonator gap g. In figure 6, a higher Q_r values mean lower radiation levels. From these results, the optimal resonator gap g is 0.3 mm. A SORR with $g = 0.3$ mm offers both a current density reduction effect of 23.2 %, as well as an improved Q_r value of 32 000, which is more than twice that of the conventional open-ring resonator. Moreover, this SORR achieves a Q_u value of 48 100.

4. Design and fabrication of prototype filter

4.1. Filter design

A prototype 5-GHz HTS-RTF is designed around the SORR to achieve, as the first step, a sharp skirt property and low IMD characteristic; filter bandwidth and suppression

levels will be tackled later. The filter is assumed to operate in the 5-GHz band, assuming its use as a transmitting filter in the next generation IMT-Advanced mobile base stations.

The design parameters are a stopband centre frequency f_c of 4.95 GHz, a 3 dB bandwidth of 1.5 MHz (fractional bandwidth = 0.03 %) and a three-pole Chebyshev response with 0.01 dB ripple. The SORR with resonator gap $g = 0.3$ mm is used in the filter design, because it offers low current densities in the passband and high-Q_u values as well as low radiation levels. The spacing between the resonator and the feedline is determined by using the resonators' normalized reactance slope parameters as calculated from the frequency responses of a single resonator [16]. The numerical analysis considered the material constants in table 1 and the shielded box shown figure 4. The geometry of the designed 5-GHz three-pole HTS-RTF is shown figure 7. The dimensions of the substrate are 20 mm $\times$ 30 mm. The long dashed lines in figure 8 show the analyzed frequency characteristics. The calculated results are $f_c = 4.95$ GHz with 3 dB bandwidth of 1.42 MHz.

4.2. Fabrication and measured S-parameter response

The designed filter is fabricated with double-sided YBCO thin films deposited on a 0.5 mm thick MgO substrate. Figure 9 shows the photograph of the fabricated filter. As shown in the dashed and solid lines in the figure 8, the S-parameter response is measured at 50 K using an Agilent 8510C network analyzer. The filter has a stopband centre frequency f_c of 4.945 GHz and a 3 dB bandwidth of 1.78 MHz. In addition, the maximum passband loss is below 0.1 dB, and the skirt slope is better than 60 dB MHz^{-1} at band edges. These characteristics, low insertion loss and sharp skirt slope, are impossible to achieve with dielectric resonators with unloaded Q-factor of around 20 000.

It is important to avoid unwanted coupling between the resonators. Since the radiation from the resonators is well suppressed, the calculated and measured results are in good agreement regarding existence of three-pole in the stopband and skirt properties. The 5 MHz frequency shift is mainly due to variation in the dielectric constant of the MgO substrate. We can obtain the same stopband centre frequency using the relative dielectric constant of 9.7211. To achieve better agreement between the analyzed and the measured stopband centre frequencies, this dielectric constant should be used for designing the filter on the wafer. In addition, the difference in the ripple in the stopband and the bandwidth is caused by minute differences in the fabricated dimensions. From the sensitivity analyses based on the single SORR, the resonance frequency of the SORR with resonator gap $g = 0.3$ mm is varied at 129 kHz per 0.1 μm of outer diameter. As a result, the resonance frequencies of three resonators are changed due to slight variations in the dimensions. This leads to a difference of 360 kHz in the bandwidth and the shape of the ripple in the stopband.

The measured $|\mathrm{S}_{11}|$ parameter is different from the analysis results in terms of the

following points: the upper reflection zero has disappeared and the level of reflection is approximately 15 dB higher. To investigate the reason, the sensitivity analyses based on the HTS-RTF shown in figure 7 are carried out. Figure 10 shows the analysis results of the $|S_{11}|$ parameters when the outer diameter of resonator No. 1 is changed at + 0.2 μm and - 0.2 μm. It is confirmed that the upper refection zero is obscured at + 0.2 μm and disappears at - 0.2 μm. In addition, figure 11 shows the analysis results when the outer diameter of resonator No. 2 is changed at + 0.2 μm and - 0.2 μm. As shown in the figure, the reflection level of the lower frequency side has increased about 10 dB at + 0.2 μm. From these results, it is found that the $|S_{11}|$ parameter is also sensitive to the tolerances in dimensions. The slight variations in the fabrication impact on frequency characteristics. With respect to the level of reflection, the difference is also due to mismatching of the contact between the coaxial connecter and the feedline. Due to these reasons, the analyzed and the measured $|S_{11}|$ parameters are different.

5. Nonlinear distortion measurements based on two-tone signal

To confirm the low IMD characteristic of the fabricated HTS-RTF, third-order and fifth-order IMD generated by the filter are measured at 50 K. The experimental setup is shown in figure 12. Figure 13 explains the two conditions under which the IMD is measured. In-band (stopband) measurements and out-of-band (passband) measurements are carried out.

The in-band measurements assumed a fundamental signal (passband signal) of 40 dBm. The adjacent channel noise (stopband signal) is -50 to -40 dBc lower than the fundamental signal, as explained in the previous section. In this case, a 500 kHz separated two-tone signal is input at the stopband centre frequency. The results of the in-band measurements are shown in figure 14(a). They shows that the third-order IMD (IMD3) is below the noise floor for the stopband signal of -10 dBm, and -66.0 dBc at the stopband signal of 0 dBm. In addition, fifth-order IMD (IMD5) is below the noise floor (about -90 dBm) for stopband signals of up to 0 dBm.

The out-of-band measurements assumed that the fundamental signal (passband signal) is input at 5 MHz above offset from the 3 dB band edge. In this case, a 500 kHz separated two-tone signal is also input. This two-tone signal passes through the filter with a loss of less than 0.1 dB. The results of the out-of-band measurements are shown in figure 14(b). They show that IMD3 is -56.7 dBc for the passband signal of 40 dBm. In addition, IMD5 is below the noise floor for passband signals of up to 42.3 dBm.

The measurements made using a two-tone continuous wave reflect different conditions from those of actual operating signals as shown in figure 1, however, the aim of this measurement is to investigate typical IMD characteristics of an HTS-RTF. These results confirm the low IMD characteristics of the HTS-RTF for both weak adjacent channel noise (stopband signal) and strong fundamental signals (passband signal).

6. ACLR measurements based on Wideband CDMA four-carrier signal

To examine the ability of the fabricated HTS-RTF to handle actual W-CDMA signals, W-CDMA four-carrier measurements are carried out. The ACLR specified in 3GPP TS 25.141 [14] is measured with and without the HTS-RTF. The ACLR definition according to the specification [14] is the ratio of the average power centred on the assigned channel frequency to the average power centred on an adjacent channel frequency.

The experimental setup is shown in figure 15. The W-CDMA four-carrier signal (3GPP test model-1) is created by the vector signal generator, which is controlled by the Agilent technologies advance design system 2006A [17]. As described in the previous section, ACLR degradation is mainly caused by the nonlinear characteristics of the transmitting power amplifiers. Strong nonlinear characteristics lead to low ACLR values. To investigate the ACLR improvement offered by the HTS-RTF, the filter is connected just after a power amplifier. Figure 16 shows the frequency arrangement of the measurements. The frequency of the W-CDMA four-carrier signal is chosen so that the upper edge of the adjacent channel and that of the upper 3 dB band edge of the HTS-RTF are the same. In addition, total output powers of up to 40 dBm are tested.

Figure 17 shows a typical power amplifier output spectrum with and without HTS-RTF. It is clear that adjacent channel noise is suppressed by more than 10 dB by the HTS-RTF. In addition, the W-CDMA signal spectrum is not altered by the filter. The HTS-RTF eliminates the noise without impacting the signal. The ACLR improvement effect is shown in figure 18. The maximum ACLR improvement is 11.0 dB and the average improvement between output powers of 20 dBm to 40 dBm is 9.8 dB. Note that this ACLR is evaluated for the bandwidth of 1.78 MHz, which is the same as the 3 dB bandwidth of the HTS-RTF. Actual bandwidth used in the evaluation of the specification [14] is 3.84 MHz, however, these results still confirm the ACLR improvement effect offered by the HTS-RTF. Furthermore, this ACLR improvement is constant up to the maximum output power tested here, 40 dBm. This means that the IMD generated by the HTS-RTF is negligible compared to that generated by the power amplifier. A fabricated HTS-RTF with bandwidth of more than 3.84 MHz should offer an ACLR improvement of more than 10 dB.

These results indicate that applying this HTS-RTF to a transmitting circuit allows us to obtain the same ACLR value at higher output powers that is possible with conventional approaches. Replacing conventional nonlinear compensation techniques with this HTS-RTF will yield transmission circuits that offer high cost performance and a low energy operation.

7. Conclusion

A new filter configuration that is capable of offering both high-power handling capability and sharp cutoff characteristics was presented. As an application example, a 5-GHz HTS-RTF based on the SORR was designed and fabricated on MgO substrates and its

feasibility was confirmed. The SORR, which can achieve low induced current densities in the passband and high-Q_u values as well as low radiation levels, was described. The measured S-parameter confirmed the existence of three-pole in the stopband. In addition, the sharp skirt properties of the $|S_{21}|$ parameter, which are the most important characteristics for the suppression of the ACLR, were in agreement with the numerical analysis results. However, the stopband centre frequency was shifted due to the variation in the dielectric constant. Regarding the bandwidth and the out-band response, the minute difference in the fabrication affected these characteristics. This resulted in the difference between the analysis results and the measured results.

Assuming the existence of weak adjacent channel noise and strong fundamental signals, the IMD characteristics of the HTS-RTF were measured using a two-tone continuous wave. The measurements showed IMD3 of -56.7 dBm at 5 MHz offset from the 40 dBm passband signal. In addition, ACLR measurements using an actual W-CDMA four-carrier signal were carried out. The ACLR was improved by about 10 dB for output powers of up to 40 dBm (the evaluated bandwidth was narrower than the specification). A very important finding is that the HTS-RTF can suppress the noise without any signal attenuation. From these results, we can conclude that the HTS-RTF is an effective way of overcoming the weak power-handling capability of existing HTS transmitting filters.

As a first step, we focused here on the sharp skirt property and low IMD levels. Next step will be to improve the filter's performance such as bandwidth and level of suppression. For the HTS-RTF to be applied to a W-CDMA mobile base station, it must offer the suppression bandwidth of at least 3.84 MHz. Noise that is not close to the carrier signal can be suppressed by using both an HTS-RTF and a conventional room temperature filter.

Acknowledgments

This work is partly supported by "Research and development of fundamental technologies for advanced radio frequency spectrum sharing in mobile communication systems" from the Ministry of Internal Affairs and Communications (MIC) of Japan.

References

[1] Lancaster M J 1997 *Passive Microwave Device Applications of High-Temperature Superconductors* (Cambridge: Cambridge University Press)
[2] Mansour R R, Ye S, Dokas V, Jolley B, Tang W C and Kudsia C M 2000 *IEEE Trans. Microwave. Theory Tech.* **48** 1199–207
[3] Hong J S, Lancaster M J, Jedamzik D, Greed R B and Mage J C 2000 *IEEE Trans. Microwave. Theory Tech.* **48** 1240–6
[4] Tsuzuki G, Ye S and Berkowitz S 2003 *IEEE Trans. Appl. Supercond.* **13** 261–4
[5] Narahashi S, Satoh K, Kawai K, Koizumi D and Nojima T 2006 *Supercond. Sci. Technol.* **19** S416–22
[6] Zhang Q *et al* 2007 *IEEE Trans. Appl. Supercond.* **17** 922–5

[7] Dahm T and Scalapino D J 1997 *J. Appl. Phys.* **81** 2002–9
[8] Sato H, Cho K, Kurian J and Naito M 2003 *Supercond. Sci. Technol.* **16** 1503–7
[9] Futatsumori S, Hikage T and Nojima T 2006 *Electron. Lett.* **42** 428–30
[10] Futatsumori S, Hikage T, Nojima T, Akasegawa A, Nakanishi T and Yamanaka K 2007 *Electron. Lett.* **43** 956–7
[11] Futatsumori S, Hikage T and Nojima T 2007 *Proc. 6th Int. Kharkov Symp. on Physics and Engineering of Microwaves, Millimeter and Submillimeter Waves and Workshop on Terahertz Technologies* (Kharkov) vol 1 398–400
[12] Nojima T and Konno T 1985 *IEEE Trans. Veh. Tech.* **34** 169–77
[13] Narahashi S and Nojima T 1991 *Proc. IEEE Int. Conf. on Communications* (Denver, CO) vol 3 1485–90
[14] Third Generation Partnership Project 2004 *3GPP TS-25.141 V6.8.0 (2004-12)* (Valbonne: Third Generation Partnership Project)
[15] Helaoui M, Boumaiza S, Ghazel A and Ghannouchi F M 2006 *IEEE Trans. Microwave. Theory Tech.* **54** 1396–404
[16] Matthaei G L, Young L and Jones E M T 1980 *Microwave Filters, Impedance-Matching Networks, and Coupling Structures* (Norwood, MA: Artech House Publishers)
[17] Agilent Technologies 2002 *Application Note 1394 Connected Simulation and Test Solutions Using the Advanced Design System* (Palo Alto, CA: Agilent Technologies)

Tables and table captions

Table 1. The material constants of MgO substrate, YBCO thin-film, and the shielded box used for numerical analysis.

Substrate: MgO	Relative dielectric constant	9.7
	Loss tangent	5.5×10^{-6}
	Thickness (mm)	0.5
HTS thin-film: YBCO	Conductivity (S/m)	6.5×10^{12}
	Thickness (μm)	0.5
Shielded box: Copper	Conductivity (S/m)	1.03×10^{9}

Figure captions

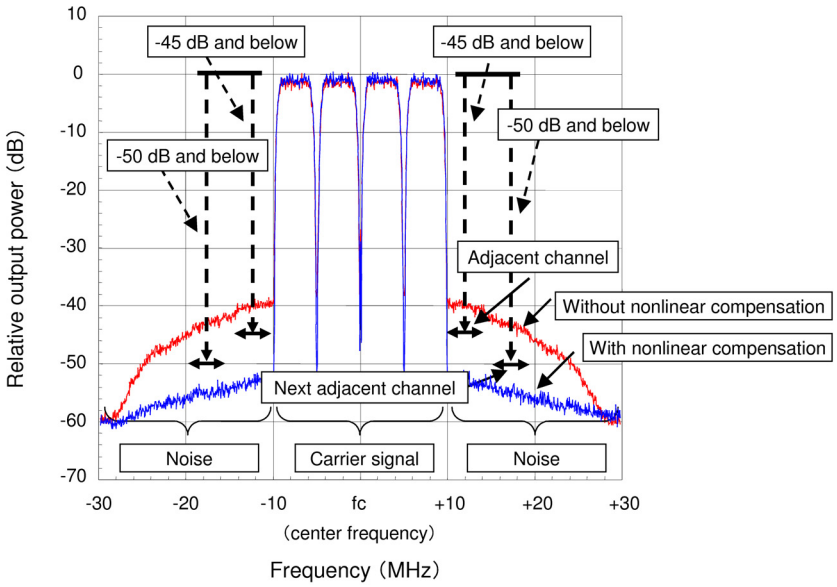

Figure 1. Typical output spectrum of a power amplifier used in a mobile base station. Wideband CDMA four-carrier output signals with and without nonlinear compensation circuits are shown. In addition, required adjacent channel leakage power ratio (follows the specification [14]) is added to the figure.

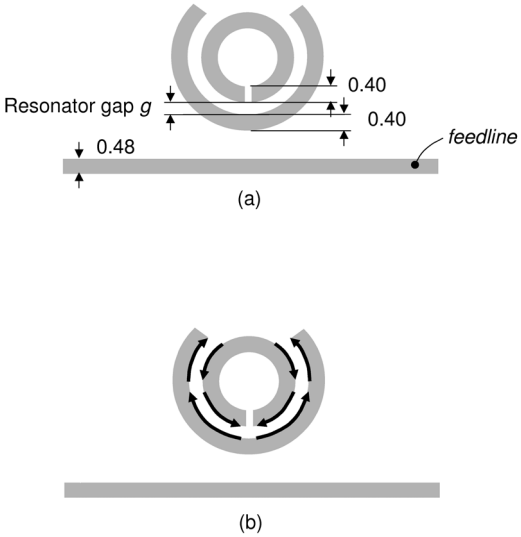

Figure 2. (a) Structure of split open-ring resonator. (all dimensions in millimetres) (b) The arrows represent the simple current flow on interior edges of the resonator elements. Note that radiation is cancelled by inverse direction currents.

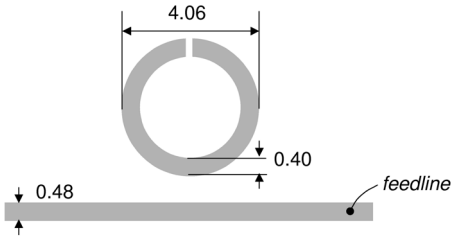

Figure 3. Structure of conventional open-ring resonator. (all dimensions in millimetres)

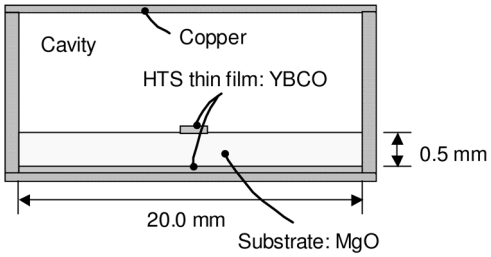

Figure 4. Structure of shielded box used for both numerical analysis and fabrication of the HTS filter.

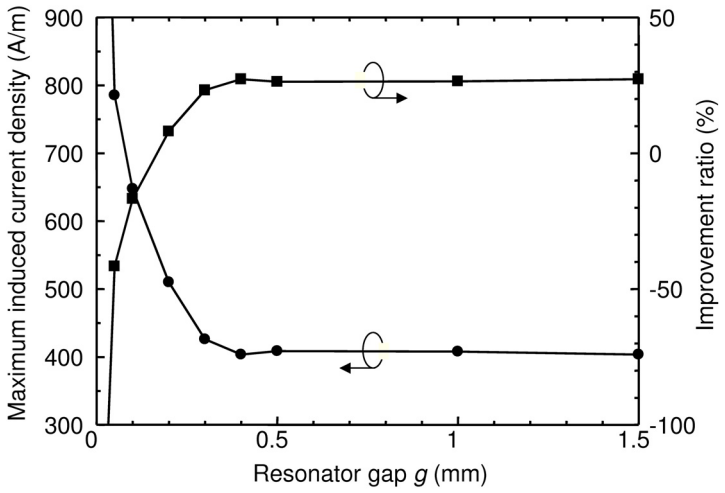

Figure 5. Maximum induced current density as a function of resonator gap g between two resonator elements. The closed circles represent maximum current density induced by a sinusoidal wave with 1 V amplitude and 5 MHz offset from the resonance frequency. The closed boxes are ratio improvements relative to the value of 554.5 A/m, which is maximum induced current density of the conventional open-ring resonator.

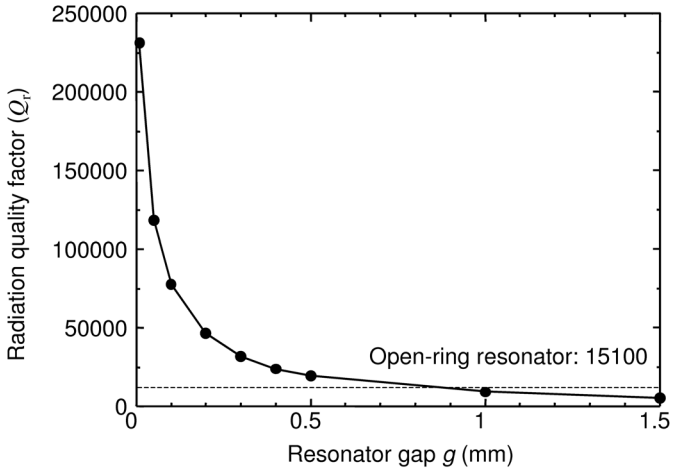

Figure 6. Radiation quality factor Q_r as a function of resonator gap g. The dashed horizontal line represents radiation quality factor of the conventional open-ring resonator.

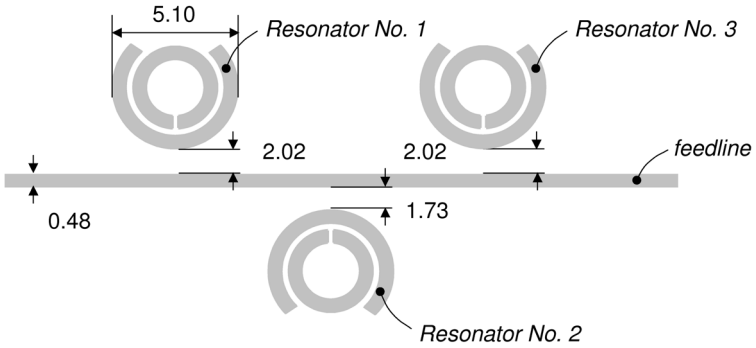

Figure 7. Structure of 5-GHz three-pole HTS reaction-type filter consisting of split open-ring resonator. (all dimensions in millimetres) The split open-ring resonator with resonator gap $g = 0.3$ mm is used as the filter.

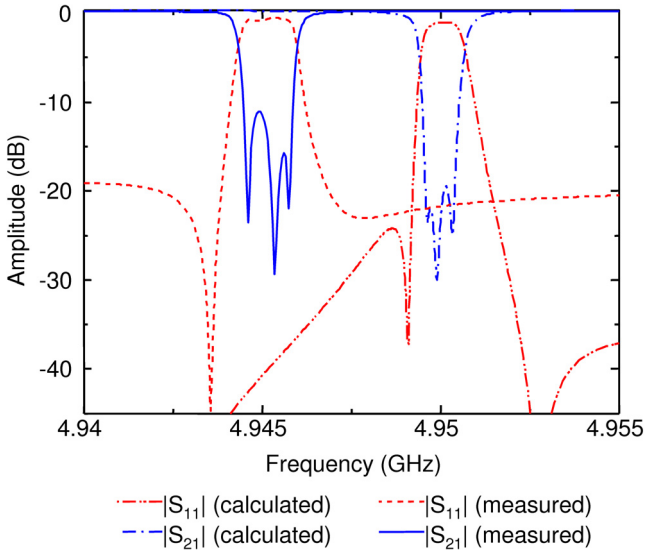

Figure 8. S-parameter responses of 5-GHz three-pole HTS reaction-type filter. The long dashed double-short dashed and long dashed short dashed lines represent $|S_{11}|$ and $|S_{21}|$ obtained by numerical analysis, respectively. In addition, the dashed and solid lines represent $|S_{11}|$ and $|S_{21}|$ measured at 50 K, respectively.

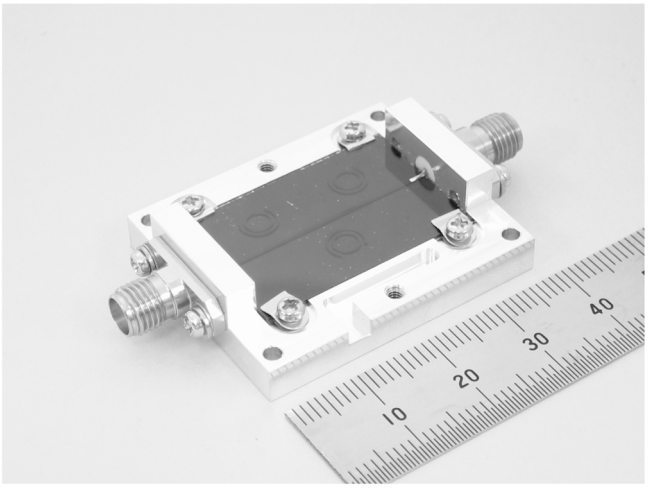

Figure 9. Photograph of fabricated filter with a top cover removed.

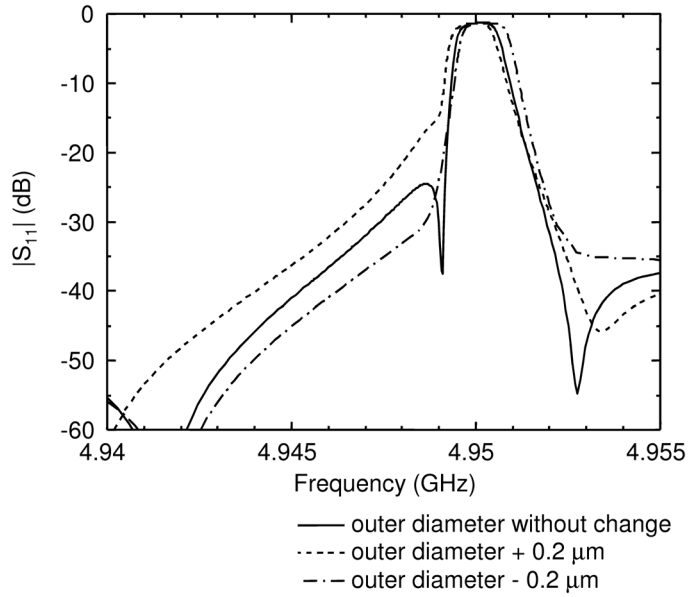

Figure 10. The analysis results of the $|S_{11}|$ parameters when the outer diameter of resonator No. 1 is changed at + 0.2 μm and - 0.2 μm. The solid line represents the value when the diameter of resonator is unchanged. In addition, the dashed and long dashed short dashed lines represent $|S_{11}|$ when the diameter of resonator is changed at + 0.2 μm and - 0.2 μm, respectively.

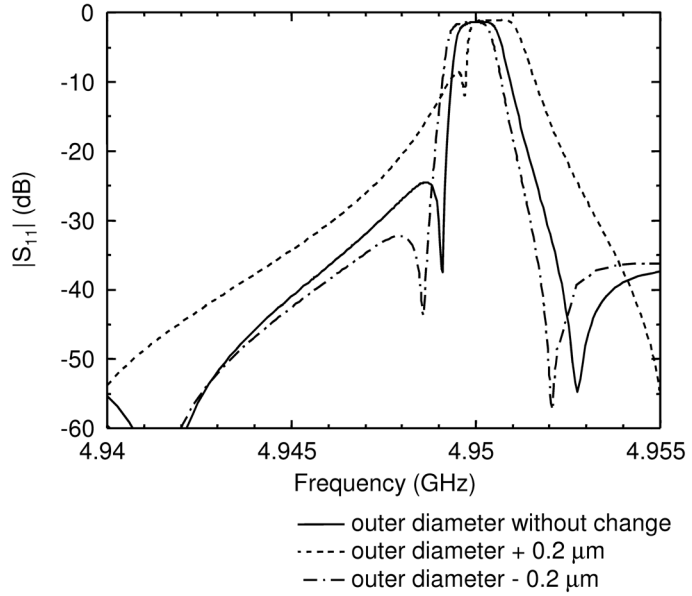

Figure 11. The analysis results of the $|S_{11}|$ parameters when the outer diameter of resonator No. 2 is changed at + 0.2 μm and - 0.2 μm. The solid line represents the value when the diameter of resonator is unchanged. In addition, the dashed and long dashed short dashed lines represent $|S_{11}|$ when the diameter of resonator is changed at + 0.2 μm and - 0.2 μm, respectively.

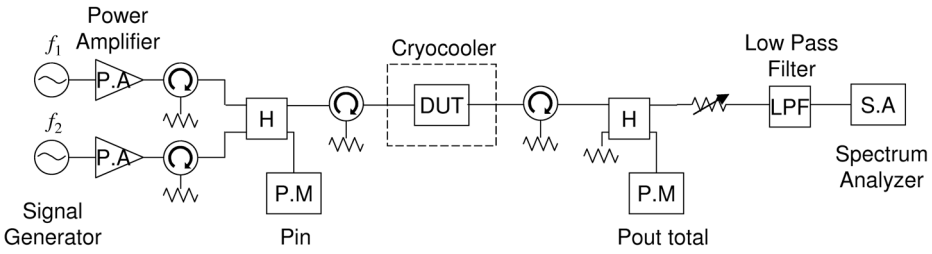

Figure 12. Schematic diagram of an experimental setup for intermodulation distortion measurements using two-tone signal on 5-GHz three-pole HTS reaction-type filter, denoted by DUT.

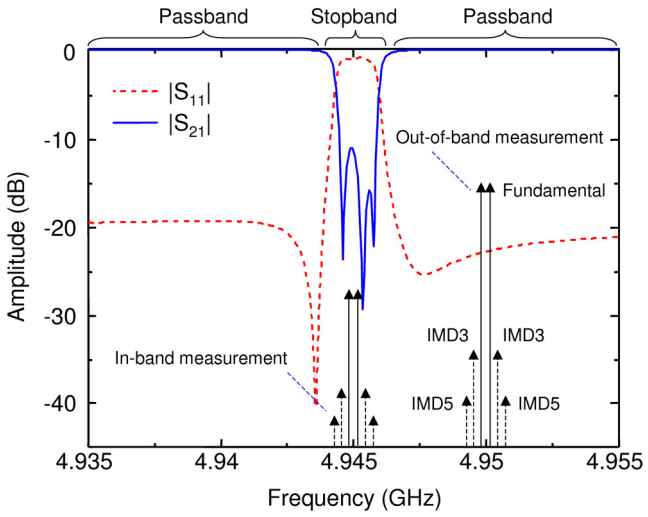

Figure 13. Two conditions of intermodulation distortion measurements are shown on the measured S-parameter response. Two-tone signal is input at the centre of stopband region in the in-band measurements. In addition, the signal is input in the passband region (5 MHz above offset from the 3 dB band edge) in the out-of-band measurements.

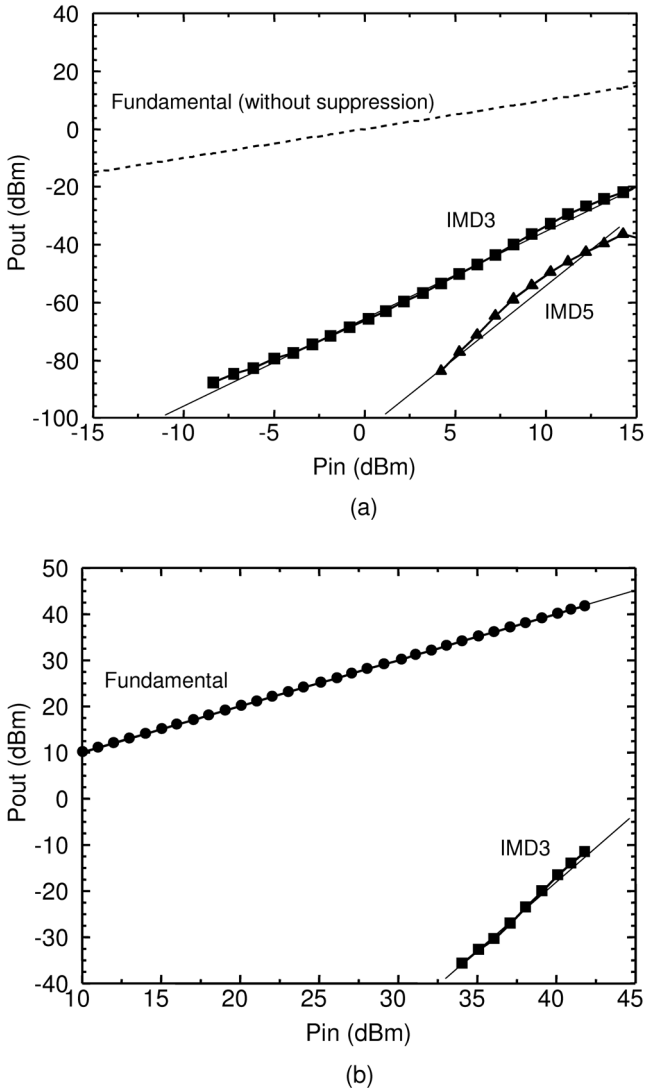

Figure 14. Measured intermodulation distortion values of (a) in the stopband region and (b) in the passband region. The closed circles represent the amplitude of the fundamental signal. In addition, the closed boxes and closed triangles represent the amplitudes of IMD3 and IMD5, respectively. (The solid straight lines are the fitting results for the fundamental signal, IMD3, and IMD5 with slopes of 1, 3, and 5, respectively.)

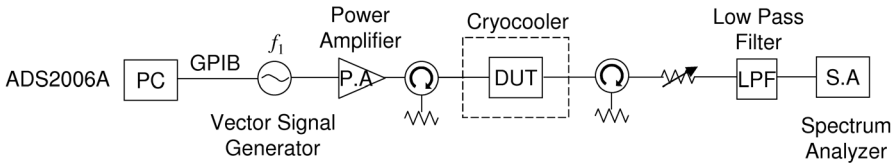

Figure 15. Schematic diagram of the experimental setup for adjacent channel leakage power ratio measurements using Wideband CDMA four-carrier signal on 5-GHz three-pole reaction-type filter, denoted by DUT. ADS2006A stands for Agilent technologies advanced design system 2006A, which provided base band I/Q signal to vector signal generator.

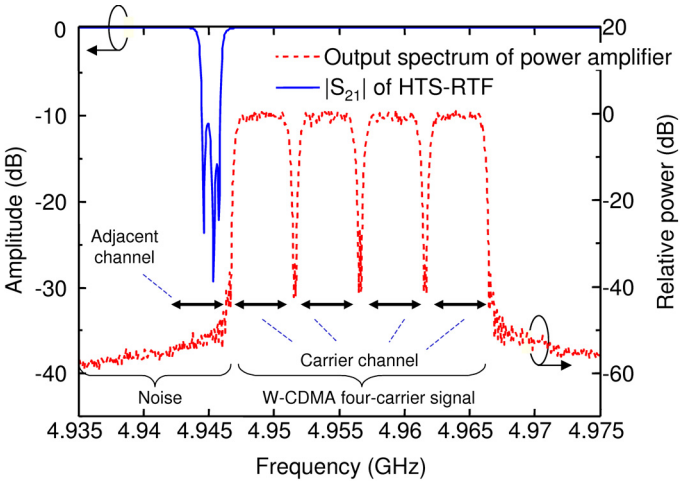

Figure 16. Condition of adjacent channel leakage power ratio measurements is shown on the measured $|S_{21}|$ response. Wideband CDMA four-carrier signal is input so the upper edge of adjacent channel and upper 3 dB band edge of the 5-GHz three-pole HTS reaction-type filter share the same frequency.

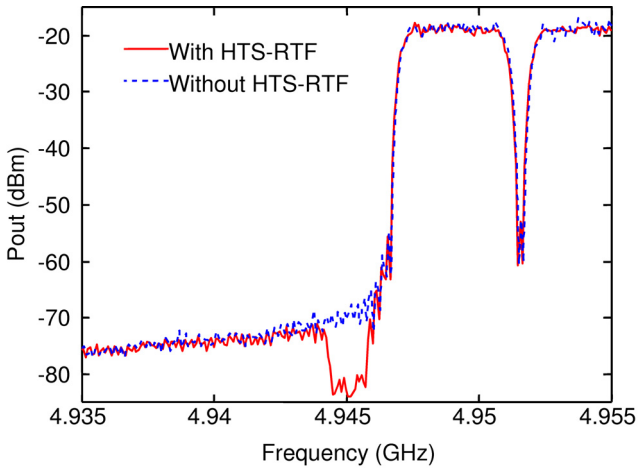

Figure 17. Typical measured output spectrum of the power amplifier; from adjacent channel leakage power ratio measurements. The solid and dashed lines represent the output spectrum with and without the 5-GHz three-pole HTS reaction-type filter, respectively.

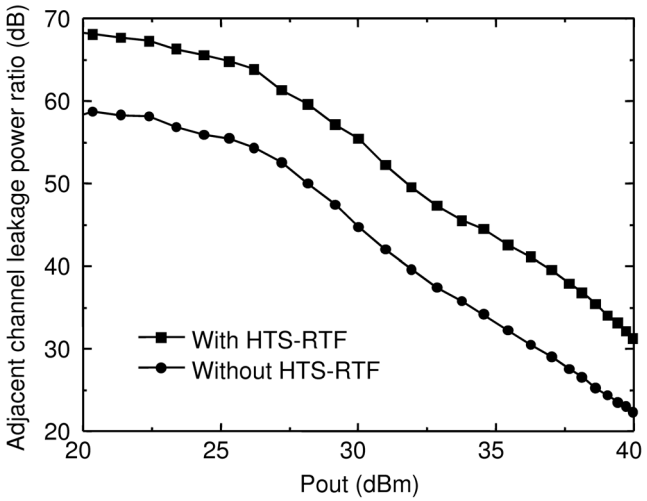

Figure 18. Measured adjacent channel leakage power ratio (ACLR) values as a function of the amplifier output power. The closed boxes represent improved ACLR values achieved with the HTS-RTF. In addition, the closed circles represent ACLR values without the HTS-RTF. Note that these ACLR values are for evaluated bandwidth of 1.78 MHz (actual evaluation bandwidth in the specification [14] is 3.84 MHz).